coatings

IMPACT FACTOR 3.4

CITESCORE 4.7

Article

Epitaxial Growth of AlN on (0001) Sapphire: Assessment of HVPE Process by a Design of Experiments Approach

Raphaël Boichot, Danying Chen, Frédéric Mercier, Francis Baillet, Gaël Giusti, Thomas Coughlan, Mikhail Chubarov and Michel Pons

Special Issue
Chemical Vapor Deposition

Edited by
Prof. Dr. Mingheng Li

MDPI

https://doi.org/10.3390/coatings7090136

coatings

MDPI

Article

Epitaxial Growth of AlN on (0001) Sapphire: Assessment of HVPE Process by a Design of Experiments Approach

Raphaël Boichot [1,*], Danying Chen [1,2], Frédéric Mercier [1], Francis Baillet [1], Gaël Giusti [3], Thomas Coughlan [1], Mikhail Chubarov [1] and Michel Pons [1]

1 Laboratoire de Science et Ingénierie des Matériaux et Procédés (SIMAP), Grenoble INP, Domaine Universitaire, 38042 Saint Martin d'Hères, France; danying.chen@simap.grenoble-inp.fr (D.C.); frederic.mercier@simap.grenoble-inp.fr (F.M.); francis.baillet@simap.grenoble-inp.fr (F.B.); tbc20@uclive.ac.nz (T.C.); mikhail.chubarov@gmail.com (M.C.); michel.pons@simap.grenoble-inp.fr (M.P.)

2 Sino-French Institute of Nuclear Engineering and Technology, Sun Yat-sen University, Zhuhai Campus, Zhuhai 519082, China

3 Sil'Tronix Silicon Technologies, 382 rue Louis Rustin, 74160 Archamps, France; gael.giusti@sil-tronix-st.com

* Correspondence: raphael.boichot@simap.grenoble-inp.fr; Tel.: +33-476-826-537; Fax: +33-476-826-677

Received: 27 July 2017; Accepted: 14 August 2017; Published: 1 September 2017

Abstract: This study aims to present the interest of using a design of experiments (DOE) approach for assessing, understanding and improving the hydride vapor phase epitaxy (HVPE) process, a particular class of chemical vapor deposition (CVD) process. The case of the HVPE epitaxial growth of AlN on (0001) sapphire will illustrate this approach. The study proposes the assessment of the influence of 15 process parameters on the quality or desired properties of the grown layers measured by 9 responses. The general method used is a screening design with the Hadamard matrix of order 16. For the first time in the growth of AlN by CVD, a reliable estimation of errors is proposed on the measured responses. This study demonstrates that uncontrolled release of condensed species from the cold wall is the main drawback of this process, explaining many properties of the grown layers that could be mistakenly attributed to other phenomena without the use of a DOE. It appears also that the size of nucleation islands, and its corollary, the stress state of the layer at room temperature, are key points. They are strongly correlated to the crystal quality. Due to the intrinsic limitations of the screening design, the complete optimization of responses cannot be proposed but general guidelines for hydride (or halogen) vapor phase epitaxy (HVPE) experimentations, in particular with cold wall apparatus, are given.

Keywords: AlN; epitaxial growth; DOE approach; HVPE; CVD

1. Introduction

AlN films have a large number of attractive properties including a high thermal conductivity, high resistivity, wide band-gap and high chemical resistance [1]. Furthermore, AlN has promising applications in surface acoustic wave devices (SAW) and microelectromechanical systems (MEMS) due to its high acoustic velocity and piezoelectric properties [2], which are maintained at high temperatures [3,4]. The most attractive perspective for AlN-base devices is in the field of deep-ultraviolet light-emitting diodes working at extremely short wavelengths [5]. For this last application, the most serious challenge is the reduction of defect density in thin films grown on foreign substrates, which limits both efficiency and reliability of the devices [6,7]. Different methods have been used to grow AlN with a low dislocation density such as physical vapor transport (PVT) [8], solution growth [9], thermal nitridation [10], metalorganic chemical vapor deposition (MOCVD) [11]

and hydride (or halogen) vapor phase epitaxy (HVPE) [12,13]. The most successful methods to provide substrates of high structural quality are the PVT method [8] or a combination of PVT and HVPE methods [14,15]. They provide AlN substrates with low dislocation densities (<10^4 cm^{-2}) able to be used for AlGaN-based deep UV light-emitting devices. Despite major progress made in the fabrication of high quality bulk AlN substrates, large-size substrates are not yet easily available. AlN films grown on foreign substrates are an intermediate choice for the fabrication of AlN-based devices. Sapphire substrates have been preferentially used because they are economical and highly transparent to UV light. AlN layers grown by HVPE on sapphire exhibit high dislocation densities (>10^8 cm^{-2}) caused by lattice and thermal expansion mismatches. Moreover, the surface mobility of aluminum is low when compared to other group III-materials [16,17].

In most recent papers [17–28] dealing with HVPE growth of AlN at high temperature from chlorinated precursors, intense efforts have been made to reduce defect densities caused by stress [29–31] before optimizing optical properties [18]. In situ etching to control void formation and stress release [17], multi-step methods to control island coalescence [32–34] or N/Al ratio [33,35], pulse injection of precursors [36], substrate position in turbulent flow [37] have been proposed to reduce strain, high dislocation densities and the appearance of cracks. The results are generally characterized by Raman spectrometry and the shift of the $E_2(h)$ phonon peak and by full width at half maximum (FWHM) values of X-ray rocking curves for tilt and twist components of the hexagonal crystal structure. These data allow the determination of mean values of residual stress. For all reactor designs and all optimized conditions by the authors [18–28], FWHM values were in the range of 100 to 600 arcsec and 500 to 800 arcsec for on-axis and off-axis peak, respectively. It is clear that the optimal temperature range is 1200–1400 °C to increase the Al mobility on the surface while avoiding sapphire degradation and/or etching [38]. Very recently, attempts to reduce strain by lateral epitaxial growth (LEO) have been proposed [21,26,34,39]. The common LEO developed for GaN has been difficult to adapt to AlN films. The masking materials commonly used do not demonstrate the same growth selectivity. The Al atoms stick to the masking materials and nucleate polycrystalline growth. The approach consists in growing films on substrates possessing elevated mesas separated by lower trench regions to promote dislocation bending [39]. Despite lateral growth and coalescence over the mesas or pillars [21,34], only one order of magnitude reduction in the threading dislocation density were observed (10^9 to 3×10^8/cm^2). The observations that can be made in all these studies is the difficulty to have a good knowledge of the actual N/Al ratio at the substrate-gas interface strongly dependent on the reactor design, supersaturation just above the substrate [40,41] and many other parameters related to the evolution of stress during the growth.

We have already proposed a modeling route involving heat and mass transfer to calculate the actual values of N/Al ratio and supersaturation just above the substrate to overcome the influence of reactor design and give guidelines on species fluxes near the reactive surface [40]. Although this modeling approach gave valuable results to better understand the intricate mixture of chemistry and fluid dynamics [42–44], it is limited by the description of boundary conditions and initial state that cannot take into account many process parameters for reasons of simplicity or computer possibility.

To complement the modeling approach, the design of experiment method (DOE) (more precisely the screening method or Plackett–Burman two level design) is applied in this study to extract the influence of the process parameters around a working growth recipe (central point). The screening method will consist (i) in varying all the recipe parameters at each experiment according to a Hadamard matrix of order 16 (15 parameters will be allowed varying in this study), and (ii) in measuring the desired properties (or responses) of the grown epitaxial layer. To date, for optimizing III-V compounds grown by CVD, only one paper dealing with this method was published [45]. The study will particularly focus on parameters for which their influence on deposition morphology is impossible to model or which present unclear effects regarding our previous studies [12–42]. Also, the assessment of the influence of the injection mode of reactive gas on the crystal quality will be studied. Rather than trying to fully optimize responses for few influencing parameters, which could be a future industrial

output, we aim to understand the influence of many parameters common to HVPE processes of AlN that were never statistically assessed in the literature. This is by definition the first step of a DOE.

The method, sequential by essence, will consist in three experimental steps or group of experiments:

- Running three times the same experiment on a central working recipe with fixed 15 parameters to quantify the error on various responses (detailed below);
- Running 16 experiments following levels indicated by an Hadamard matrix of order 16 for each parameter and measuring the responses;
- Running 1 additional experiment on the central working recipe (to assess any shifting of process) and one final experiment with all the parameters in a configuration out of Hadamard matrix to assess the robustness of the simple linear model obtained.

The influence of each parameter on each response will be discussed. A special focus will be made on the stresses of grown layers. All experiments and characterizations are performed in a limited amount of time (3 months) with the same apparatus and the same trained operator. It is assumed that the absolute experimental error is constant across the explored space of parameters.

2. Method

High temperature CVD apparatus studied is the vertical silica cold wall reactor with graphite substrate holder heated by induction depicted in Figure 1. The total height of the CVD reactor is approximately 1 m.

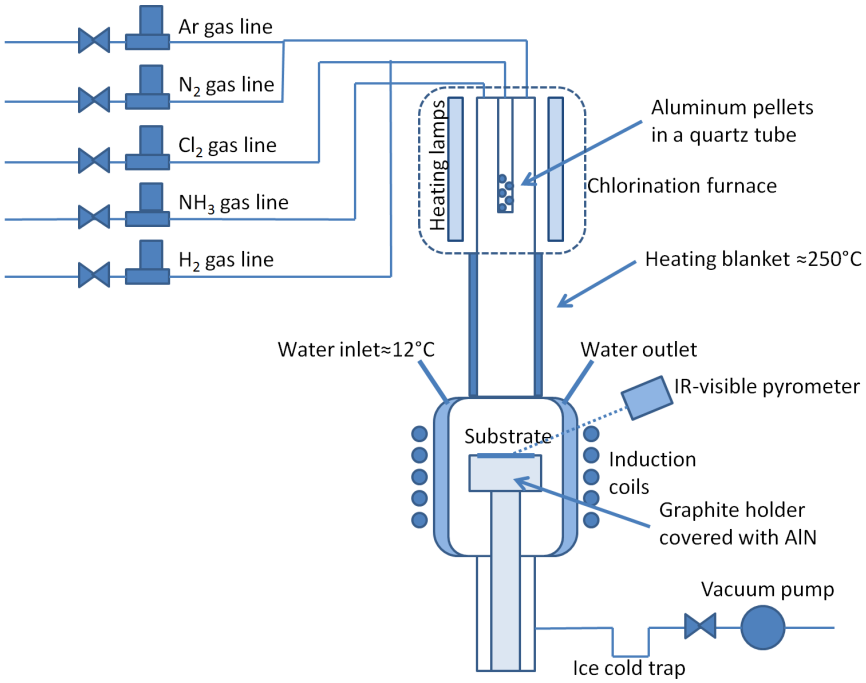

Figure 1. Vertical cold wall CVD reactor used in this study. System of valves used for pulsing is not depicted for sake of clarity.

Our reactor is composed of a chlorination chamber and a growth chamber. All the gases have a purity of 99.999%. We use NH_3 for nitrogen source and $AlCl_3$ for aluminum source. $AlCl_3$ is produced by direct chlorination of aluminum pellets (Goodfellow Company, Coraopolis, PA, USA, purity of 99.999%) with Cl_2 in the chlorination furnace. The amount of aluminum (≈5 g) is kept constant between experiments and the chlorination furnace temperature is controlled by the power of

the lamp furnace (typically around 550 °C). Substrates are 2" epi-ready c-plane sapphire supplied by The Roditi International Corporation Ltd., London, UK.

A typical working recipe is designed as followed:

- The chlorination furnace is loaded with the same mass of aluminum pellets 5 or 10 mm in diameter (discrete parameter) and the substrate is loaded out of the box (no further cleaning) into the reactor body under vacuum few minutes or the day before experiments (discrete parameter to assess the effect of room temperature desorption); The aluminum pellets can be new or used once in a preceding experiment (discrete parameter).
- The reactor vessel is purged three times with argon at room temperature.
- The aluminum load is cleaned under hydrogen (200 sccm) for a time varying from 0 to 30 min at a temperature fixed by the furnace power varying from 40% to 50%, corresponding to a temperature for the aluminum pellets in the approximate range 500–600 °C.
- The pressure into the reactor is set (1330 to 2660 Pa or 10 to 20 torrs) and the flow rate of hydrogen is set to a value varying from 3.72×10^{-4}, to 1.12×10^{-3} mol·s^{-1} (500 to 1500 sccm).
- The temperature is ramped-up at 2%/min of the induction coil power (temperature increase of the substrate around 20 °C/min).
- The substrate is cleaned at 1100 °C under hydrogen for a time varying from 0 to 20 min.
- The temperature is ramped-up again at 2%/min of the induction coil power toward the deposition temperature (1200 to 1300 °C).
- Cl_2 (2 sccm or 1.49×10^{-6} mol·s^{-1}) is injected into the chlorination tube from 0 to 2 min prior to NH_3 to tentatively favor Al polarity; this step is called "pre-chlorination".
- Cl_2 and NH_3 flow rates are set to their set points (2 sccm Cl_2, 1.33 to 3.99 sccm NH_3 or 9.90×10^{-7} to 2.97×10^{-6} mol·s^{-1}, N/Al ratio in gas phase ranging from 1 to 3).
- Reactants are sequentially injected, $AlCl_3$ for one second then purge then NH_3 for one second then purge, or simultaneously injected, both at the same time for one second then purged (discrete parameter), with purge times varying from 0 to 4 s (the growth mode consequently ranging from pure "ALD-like" mode (atomic layer deposition, sequential injection with purges in-between) to CVD (simultaneous injection without purge) passing by pulsed or modulated CVD (simultaneous injection with purges or sequential injection without purges). The intake time of reactants (NH_3 and $AlCl_3$) is set to 1000 s each, so that the total mole quantity of reactants entering the reactor is kept constant between depositions.
- The gas phase is then changed to pure N_2 or H_2 + 1%NH_3, keeping the same flow rate (discrete parameter).
- The temperature is ramped-down at 1%/min or 3%/min of the induction coil power toward 600 °C.
- Final cooling down to room temperature is performed with 1000 sccm Ar.
- Sample is unloaded and reactor tube is finally cleaned with 5% HCl in deionized water, then deionized water, then isopropanol. Tube is finally dried under vacuum before next experiment.

For the experiments involving the central working recipe, the discrete parameters are set to an extreme value (±1 in normalized level), while continuous parameters take their mean central value (0 in normalized level, see header of Table 1 for details). Due to the discrete aspect of some parameters, the central working recipe does not present every parameter at level 0. For the experiments designed by the Hadamard matrix, all the parameters take their extreme values. Table 1 summarize the whole set of experiments performed in this study with the corresponding values of the parameters. Experiments #1–3, 17 are processed according to the central working recipe, experiments #4–19, 21 follow the Hadamard matrix and experiment #20 is designed to be completely out of the Hadamard matrix.

Table 1. Experimental campaign designed by the screening method following Hadamard matrix of order 16. 1 sccm = 7.44×10^{-7} mol·s^{-1}. The chronological order of experiments may not follow the order of Hadamard matrix.

Comment	Experiment #	Mounting	Pellets	Pellet Size (mm)	Pressure (Pa)	Lamp Furnace Setpoint
Central working recipe 1	1	Same day	New	5	1995	45%
Central working recipe 2	2	Same day	New	5	1995	45%
Central working recipe 3	3	Same day	New	5	1995	45%
Hadamard 1	4	Same day	New	10	2660	50%
Hadamard 2	5	Day before	Used once	10	1330	50%
Hadamard 3	6	Day before	New	10	1330	50%
Hadamard 4	7	Same day	Used once	10	2660	50%
Hadamard 5	19	Same day	New	5	1330	40%
Hadamard 6	8	Day before	Used once	5	2660	40%
Hadamard 7	9	Day before	New	5	2660	40%
Hadamard 8	10	Same day	Used once	5	1330	40%
Hadamard 9	11	Same day	New	10	1330	40%
Hadamard 10	12	Day before	Used once	10	2660	40%
Hadamard 11	13	Day before	New	10	2660	40%
Hadamard 12	14	Same day	Used once	10	1330	40%
Hadamard 13	15	Same day	New	5	2660	50%
Hadamard 14	16	Day before	Used once	5	1330	50%
Hadamard 15	21	Day before	New	5	1330	50%
Hadamard 16	18	Same day	Used once	5	2660	50%
Central working recipe 4	17	Same day	New	5	1995	45%
Out of Hadamard experiment	20	Day before	Used once	5	1330	40%
Normalized levels		Same day = +1 Day before = −1	New = +1 Used once = −1	5 = −1 10 = +1	1330 = −1 1995 = 0 2660 = +1	40% = −1 45% = 0 50% = +1

Comment	Experiment #	Aluminum Pellet Cleaning Time (min)	Substrate Cleaning Time at 1100°C (min)	Growth Temperature (°C)	$AlCl_3$ Initial Chlorination Time (min)	Injection Mode
Central working recipe 1	1	20	10	1250	1	Sequential
Central working recipe 2	2	20	10	1250	1	Sequential
Central working recipe 3	3	20	10	1250	1	Sequential
Hadamard 1	4	30	20	1300	2	Simultaneous
Hadamard 2	5	30	0	1300	2	Sequential
Hadamard 3	6	10	20	1200	2	Simultaneous
Hadamard 4	7	10	0	1200	2	Sequential
Hadamard 5	19	30	20	1200	2	Sequential
Hadamard 6	8	30	0	1200	2	Simultaneous
Hadamard 7	9	10	20	1300	2	Sequential
Hadamard 8	10	10	0	1300	2	Simultaneous
Hadamard 9	11	10	0	1200	0	Simultaneous
Hadamard 10	12	10	20	1200	0	Sequential
Hadamard 11	13	30	0	1300	0	Simultaneous
Hadamard 12	14	30	20	1300	0	Sequential
Hadamard 13	15	10	0	1300	0	Sequential
Hadamard 14	16	10	20	1300	0	Simultaneous
Hadamard 15	21	30	0	1200	0	Sequential
Hadamard 16	18	30	20	1200	0	Simultaneous
Central working recipe 4	17	20	10	1250	1	Sequential
Out of Hadamard experiment	20	10	0	1200	0	Sequential
Normalized levels		10 = −1 20 = 0 30 = +1	0 = −1 10 = 0 20 = +1	1200 = −1 1250 = 0 1300 = +1	0 = −1 1 = 0 2 = +1	Sequential = −1 Simultaneous = +1

Table 1. *Cont.*

Comment	Experiment #	NH_3 Flow Rate (sccm)	Purge Time (s)	H_2 Flow Rate (sccm)	Cooling Down Gas	Cooling Down Rate (%/min)
Central working recipe 1	1	2.66	2	1000	N_2	2
Central working recipe 2	2	2.66	2	1000	N_2	2
Central working recipe 3	3	2.66	2	1000	N_2	2
Hadamard 1	4	3.99	4	1500	N_2	3
Hadamard 2	5	3.99	0	500	N_2	1
Hadamard 3	6	1.33	0	500	H_2 + 1% NH_3	3
Hadamard 4	7	1.33	4	1500	H_2 + 1% NH_3	1
Hadamard 5	19	1.33	0	1500	N_2	1
Hadamard 6	8	1.33	4	500	N_2	3
Hadamard 7	9	3.99	4	500	H_2 + 1% NH_3	1
Hadamard 8	10	3.99	0	1500	H_2 + 1% NH_3	3
Hadamard 9	11	3.99	4	500	N_2	1
Hadamard 10	12	3.99	0	1500	N_2	3
Hadamard 11	13	1.33	0	1500	H_2 + 1% NH_3	1
Hadamard 12	14	1.33	4	500	H_2 + 1% NH_3	3
Hadamard 13	15	1.33	0	500	N_2	3
Hadamard 14	16	1.33	4	1500	N_2	1
Hadamard 15	21	3.99	4	1500	H_2 + 1% NH_3	3
Hadamard 16	18	3.99	0	500	H_2 + 1% NH_3	1
Central working recipe 4	17	2.66	2	1000	N_2	2
Out of Hadamard experiment	20	1.33	0	500	H_2 + 1% NH_3	1
Normalized levels		1.33 = −1 2.66 = 0 3.99 = +11	0 =−1 2 = 0 4 = +1	500 = −1 1000 = 0 1500 = +1	H_2 + 1% NH_3 = −1 N_2 = +1	1 = −1 2 = 0 3 = +1

All the experiments described in Table 1 led to epitaxial growth on (0001) sapphire. No disorientation is observed and AlN presents its classical orientation AlN (0001)//sapphire (0001) and AlN [10-10]//sapphire [11-20]. Cracks could be observed on the surface of some samples (see Table 2 for details).

The measured output responses quantifying the desired properties of the AlN epitaxial layers are the following:

- Raman Shift in cm^{-1} of the $E_2(h)$ peak of AlN measured far from cracks with a Renishaw In-Via spectrometer (Renishaw, Wotton-under-Edge, Gloucestershire, UK) and a 10 mW Ar^+-laser with 514 nm wavelength. The shift is averaged on 12 measurements covering the full wafer with spot diameter $\approx$1 µm.
- FWHM (Full Width at Half Maximum) of $E_2(h)$ peak of AlN measured far from cracks and averaged on 12 measurements covering the full wafer. This should be representative of the quality of AlN layer.
- Radius of curvature of the sample (in m^{-1}) measured by a Talysurf Mechanical profilometer (Ametek Inc, Berwyn, PA, USA). Orthogonal cross measurements of the whole sample were averaged.
- FWHM of the 0002 reflection peak of AlN measured by XRD measurements in ω-scan. Such measurements were performed in PANalytical X'Pert PRO powder diffractometer (PANalytical, Almelo, The Netherlands) using Cu $K_{\alpha 1,2}$ radiation.
- Thickness in nm measured by optical ellipsometry (ellipsometer Accurion, Nanofilm EP3 SE, Accurion GmbH, Goettingen, Germany).
- RA (arithmetic average) and RMS (root mean square) roughness measured by AFM (Atomic Force Microscopy). AFM measurements were performed using NanoScope Dimension 3100 (Bruker France S.A.S, Palaiseau, France) in tapping mode. The roughness are measured far from surface cracks and averaged on several scanning area of 10 µm × 10 µm.
- Finally, the size of primary nucleation islands is calculated from the stress state of the AlN layer measured at room temperature by the Raman shift or the radius of curvature.

The general method to calculate the primary nucleation island size is explained in [46]. It consists in writing a mechanical modeling of the AlN layer + sapphire substrate taking into account the initial compressive misfit strain of −0.7% [47], tensile strain due to island coalescence [48] depending on island size at coalescence and thermal strain due to the misfit in thermal expansion coefficients between materials. The polynomial used for fitting the thermal expansion coefficients of AlN and sapphire normal to *c*-axis (biaxial stress only) and their respective biaxial modulus come from different sources [49–52]. The island size at coalescence is used as the adjusting parameter so that the calculated stress fits with the stress deduced from Raman shift [53] or curvature measurements. The smaller the islands, the more important the tensile strain at room temperature is.

Table 2. Measured outputs of the screening method.

Comment	Experiment #	Raman Shift (cm^{-1})	FWHM Raman E2h (cm^{-1})	1/Radius of Curvature (m^{-1})	FWHM (0002) (arcsec)	Thickness (nm)
Central working recipe 1	1	657.5	13.0	-3.693×10^{-2}	3576	1293
Central working recipe 2	2	657.7	13.2	-3.457×10^{-2}	3684	1334
Central working recipe 3	3	657.2	11.4	-3.205×10^{-2}	3311	1242
Hadamard 1	4	657.7	10.7	-5.152×10^{-2}	4087	1741
Hadamard 2	5	656.6	12.5	-1.790×10^{-2}	1434	657
Hadamard 3	6	657.8	10.2	-6.370×10^{-3}	779	145
Hadamard 4	7	657.3	11.9	-8.270×10^{-2}	4206	1780
Hadamard 5	19	649.9	7.3	1.312×10^{-2}	355	714
Hadamard 6	8	658.1	9.9	-4.113×10^{-2}	3077	1399
Hadamard 7	9	659.1	11.0	-5.834×10^{-2}	3889	2149
Hadamard 8	10	651.7	10.7	1.067×10^{-2}	589	388
Hadamard 9	11	655.7	9.5	3.822×10^{-4}	2198	776
Hadamard 10	12	656.8	9.8	3.872×10^{-3}	1980	1226
Hadamard 11	13	655.7	10.9	1.613×10^{-3}	1130	1471
Hadamard 12	14	657.4	12.8	3.070×10^{-2}	2269	1632
Hadamard 13	15	657.2	6.7	-3.391×10^{-3}	669	284
Hadamard 14	16	658.0	11.0	-6.562×10^{-2}	5324	2355
Hadamard 15	21	653.7	7.0	2.255×10^{-2}	1133	836
Hadamard 16	18	644.6	11.8	1.039×10^{-2}	657	199
Central working recipe 4	17	656.2	10.6	-2.946×10^{-2}	2091	1183
Out of Hadamard experiment	20	656.4	7.9	-3.147×10^{-3}	1164	393

Comment	Experiment #	Roughness RMS (nm)	Roughness R_a (nm)	Island Size from Curvature (nm)	Island Size from Raman Shift (nm)	Presence of Cracks
Central working recipe 1	1	10.2	7.9	49.7	37.4	Yes
Central working recipe 2	2	7.6	6.2	48.4	38.6	Yes
Central working recipe 3	3	11.8	8.9	48.4	35.8	Yes
Hadamard 1	4	39.2	31.2	48.7	37.6	Yes
Hadamard 2	5	17.3	11	47.5	33.3	Yes
Hadamard 3	6	12.7	8.5	60.1	40.1	No
Hadamard 4	7	363	242	62.1	37.6	No
Hadamard 5	19	8.7	7	33.4	18.5	Yes
Hadamard 6	8	20.8	15	51.7	41.7	Yes
Hadamard 7	9	15.4	12.5	47.6	44.2	Yes
Hadamard 8	10	39.9	21.4	29.6	20.6	Yes
Hadamard 9	11	171	103	38.6	31.6	Yes
Hadamard 10	12	123	73	38.0	35.4	Yes
Hadamard 11	13	17.1	10	36.5	30.1	No
Hadamard 12	14	121	52.3	31.6	36.1	No
Hadamard 13	15	192	142	41.1	35.4	No
Hadamard 14	16	7.8	6.3	47.9	38.7	Yes
Hadamard 15	21	506	419	31.1	25.8	No
Hadamard 16	18	2.2	1.7	25.8	12.5	Yes
Central working recipe 4	17	10	8.5	47.9	32.8	Yes
Out of Hadamard experiment	20	11	8.8	42.0	38.5	No

3. Results

Figure 2 shows the typical aspect of the surface of an AlN sample grown epitaxial on sapphire and the corresponding XRD θ–2θ pattern (cracked sample of experiment #17).

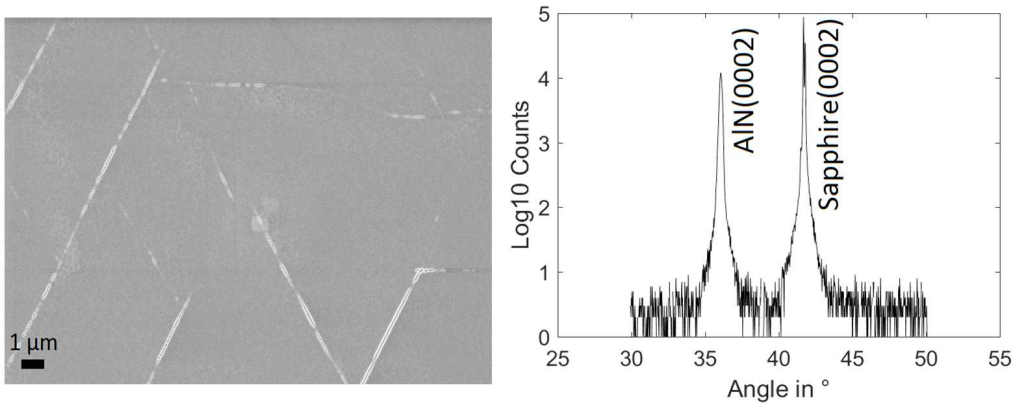

(**a**) (**b**)

Figure 2. Typical SEM surface view (**a**) and XRD θ–2θ pattern corresponding to the sample of experiment #17 (**b**).

Table 2 gives the raw values of the 9 chosen outputs and an extra column to indicate if apparent cracks are seen (by SEM) on surface. The desired properties for AlN layers is a low roughness, low FWHM of X-rays diffraction peaks, low (or compressive) stress to avoid cracks and delamination and high thickness (high growth rate).

From the experimental data, the screening method allows us to deduce the polynomial coefficients of a linear relationship between each output and the 15 varying parameters:

$$R_k = A_{k,0} + \sum_{n=1}^{15} A_{k,n} P_n$$

where R_k is the response value number k, n is a parameter number and P a parameter level (± 1). $A_{k,0}$ is the mean value of the response number k. It is convenient to reduce the parameter value so that they fit in the range $[-1,+1]$. Thus, every $A_{k,n}$ weight can be directly compared to the other. The A weights are calculated with a multi-linear fitting method under Matlab (R2016a). To assess the influence of a parameter on a response, the weight A associated to a parameter P is compared to 2 times the standard deviation (2σ) of the response evaluated with the four central working points (average of response of experiments #1, 2, 3 and 17). A weight below this limit has no statistical signification: the associated parameter does not play any significant role on the measured response within a 95% confidence interval. It should be noted that each response could be statistically analyzed since their respective averages with the 4 central working recipe experiments are well above 2 times their standard deviations. Consequently, the responses measured do not correspond to experimental noise. Table 3 presents the effect or weight of each 15 parameters on the 9 responses. For the sake of clarity, Table 3 gives the influence of each parameter on each response by levels. ($\pm$) Indicates influence just below the significance (doubtful), $\pm$ indicates influence above 2σ (certain) and $\pm\pm$ indicates influence above 3σ (strong). $-$ or + indicates a negative of positive influence of the parameter on the value (not on the desirability) of the response, regarding the coding of the normalized level.

Table 3. Level of influence of parameters on outputs or responses.

Parameter	Mounting	Pellets	Pellet Size (mm)	Pressure (Pa)	Lamp Furnace Setpoint	Aluminum Pellet Cleaning Time (min)
Raman shift (cm^{-1})	−	no effect	+	no effect	no effect	(−)
FWHM Raman E_2h (cm^{-1})	no effect	no effect	no effect	no effect	no effect	no effect
1/radius of curvature (m^{-1})	(+)	no effect	no effect	− −	− −	+ +
FWHM (0002) (arcsec)	no effect	no effect	no effect	no effect	no effect	no effect
Thickness (nm)	−	no effect	no effect	+	(−)	no effect
Roughness RMS (nm)	+ +	+ +	+	− −	+ +	− −
Roughness Ra (nm)	+	+ +	− −	− −	+ +	− −
Island size from curvature (nm)	− −	no effect	+ +	+	+ +	− −
Island size from Raman shift (nm)	no effect	no effect	no effect	no effect	no effect	no effect
Normalized levels	Same day = +1 Day before = −1	New = +1 Used once = −1	5 = −1 10 = +1	1330 = −1 1995 = 0 2660 = +1	40% = −1 45% = 0 50% = +1	10 = −1 20 = 0 30 = +1

Parameter	Substrate Cleaning Time at 1100°C (min)	Growth Temperature (°C)	$AlCl_3$ Initial Chlorination Time (min)	Injection Mode	NH_3 Flow Rate (sccm)	Purge Time (s)
Raman shift (cm^{-1})	no effect	(+)	no effect	no effect	no effect	+
FWHM Raman E_2h (cm^{-1})	no effect	no effect	no effect	no effect	no effect	no effect
1/radius of curvature (m^{-1})	no effect	no effect	− −	no effect	no effect	− −
FWHM (0002) (arcsec)	no effect	no effect	no effect	no effect	no effect	(+)
Thickness (nm)	+	++	no effect	no effect	(−)	++
Roughness RMS (nm)	− −	− −	− −	− −	++	++
Roughness R_a (nm)	− −	− −	− −	− −	++	++
Island size from curvature (nm)	no effect	no effect	++	no effect	− −	++
Island size from Raman shift (nm)	no effect	no effect	no effect	no effect	no effect	(+)
Normalized levels	0 = −1 10 = 0 20 = +1	1200 = −1 1250 = 0 1300 = +1	0 = −1 1 = 0 2 = +1	Sequential = −1 Simultaneous = +1	1,33 = −1 2,66 = 0 3,99 = +1	0 =−1 2 = 0 4 = +1

Parameter	H_2 Flow Rate (sccm)	Cooling Down Gas	Cooling Down Rate %/min	Interactions	Quadratic Effects	Mean Value	2 times Standard Deviation
Raman shift (cm^{-1})	no effect	no effect	no effect	Yes		6.5546×10^2	1.2815
FWHM Raman E_2h (cm^{-1})	no effect	no effect	no effect	No	Yes	1.0223×10	2.5260
1/radius of curvature (m^{-1})	no effect	(−)	+ +	Yes		-1.4605×10^{-2}	6.4418×10^{-3}
FWHM (0002) (arcsec)	no effect	no effect	no effect	No	Yes	2.1110×10^3	1.4665×10^3
Thickness (nm)	+ +	no effect	−	No	Yes	1.1100×10^3	1.3005×10^2
Roughness RMS (nm)	+ +	− −	+ +	Yes		1.0362×10^2	3.4807
Roughness R_a (nm)	+ +	− −	+ +	Yes		7.2261×10^1	2.3532
Island size from curvature (nm)	no effect	(+)	no effect	Yes		4.1953×10	1.5435×10^{-1}
Island size from Raman shift (nm)	no effect	no effect	no effect	Yes		3.2451×10	5.0110×10^{-1}
Normalized levels	500 = − 1 1000 = 0 1500 = +1	H_2 + 1% NH_3 = −1 N_2 = +1	1 = −1 2 = 0 3 = +1				

Experiment #20 (experiment out of Hadamard matrix) is used to establish the level of accuracy of the linear model postulated. Table 3 indicates whether interactions terms or quadratic terms may be necessary to increase the accuracy of modeling. Whatever the kind of inaccuracy, new experiments are required to establish surface response if optimization is the final aim. This extra level of analysis with new experiments leading to complete modeling of responses (factorial design) will not be developed here, Plackett–Burman two level design being sufficient to assess the effect of the parameters.

While the physical explanation of effects and main phenomena will be discussed in the next section, the effect of each parameter on each response is now described. First, it should be noted that the weight of each parameter on the FWHM of the $E_2(h)$ Raman peak is negligible ($A_{k,n} << 2\sigma$). The mean value of this parameter is 10.22 cm^{-1}. In consequence, this response does not depend on any parameter in the studied range. Moreover, we do not find any relationship between this response and the FWHM of the 0002 diffraction peak in XRD ω-scan. The size of primary islands deduced from Raman shift is also not dependent on any of the tested parameter, with a mean value of 32.4 nm and every $A_{k,n} < 2\sigma$. These two responses are in consequence excluded from further discussion in terms of parameter influence even if their measurement is statistically robust. It means that the range of variation of parameters in this study may be too small to observe any influence. However, these data are not excluded for further relationships between outputs.

The mean value of the $E_2(h)$ Raman shift peak of AlN is approximately 655.4 cm^{-1} (unstressed AlN is 657.4 cm^{-1} [54]). In consequence, according to Raman spectroscopy, AlN films are on average in a weak tensile state (0.56 GPa). Increasing pellet size and purge time during deposition as well as mounting sample the day of experiment increases $E_2(h)$ Raman shift of AlN (stress go to compressive side).

The mean value on the inverse of curvature (proportional to total stress) is −0.00146 m, indicating an average slightly compressive state of AlN film (−0.29 GPa). Increasing purge time, increasing pre-chlorination time, increasing furnace power, increasing pressure, decreasing cooling down rate and decreasing the pellet cleaning time under hydrogen increases the compressive state of the AlN layers (or decrease the tensile contribution). The effect of parameters on stress measured both by Raman spectroscopy and curvature method does not show any contradiction concerning the parameters having a shared influence on these two parameters. Surprisingly, temperature is only a second order parameter for film stress. The reason will be discussed in the next section.

The mean value of the size of primary nucleation islands deduced from the curvature of the sample is 41.9 nm (32.4 nm for the one deduced from Raman shifts). It should be reminded that smaller island size leads to pronounced tensile stress induced in AlN layers during coalescence [48]. Loading sample the day before experiment, increasing the aluminum pellet size, the pressure, the lamp furnace power set point, the pre-chlorination time and the purge time or decreasing the flow rate of NH_3 and the aluminum pellet cleaning time increases the nucleation island size. The consistency between the effect of parameters on Raman shift, inverse of curvature and island size deduced from curvature must be noted. Temperature is never influencing these parameters. This striking result will be discussed in next section.

FWHM of (0002) diffraction peak in ω-scan presents a mean value of 2111 arcsec, which is quite average in terms of crystal quality. Deceptively, no parameter seems to play a major role even if the FWHM values are contrasted (from 355 to 5324 arcsec, so a density of (screw) dislocations of 2.74×10^8 to 1.58×10^{11} cm^{-2} [13]). This is essentially due to the huge error bar at $\pm 2\sigma$ (experiment #17 present a significantly better quality than #1–3). The signification is that the main parameters influencing the crystal quality are surprisingly not embedded into this study or that the range of variation of parameters is too low. In the limit of statistical significance we can observe that the introduction of purge periods decreases the crystal quality.

The average value of the thickness of the grown layer is 1110 nm. To increase the thickness, the sample have to be mounted the day before experiment, the purge time, etching time of substrate

under hydrogen, hydrogen flow rate, temperature and pressure should be high. In the other hand, the cooling down rate should be low.

The influence of parameters on RA and RMS roughness is similar; both will be discussed at the same time on the basis of the analysis of RMS roughness only. The mean value of the RMS roughness of AlN layer in nm is 103.6 nm. The effect of every parameter is certain. Thus, this response could be easily improved (lowered) in future works. To decrease the RMS roughness, the aluminum pellets should be used once, the cooling down gas should be N_2, the gas must be injected simultaneously without purge (just as classical CVD does), the sample should be mounted the day before the experiment, pellets should be small, ammonia flow rate should be low, pre-chlorination time should be high, pellets cleaning time should be long, substrate etching time with hydrogen should be long, hydrogen flow rate should be low, furnace power should be low, cooling down rate should be low, temperature and pressure should be high. We can observe that the ALD-type injection of gases (sequential with purge time) is not interesting for decreasing the roughness. This is clearly an unexpected result that will be discussed in next section.

4. General Discussion on the Effect of Process Parameters

In order to extract general trends from experiments realized in this particular CVD reactor with the DOE method, we will try to sort out what is just technical optimization and what is of first interest for the CVD community. To do so, we will not discuss the results by parameters, nor by responses, but by driving phenomena.

First, a striking result is that within a narrow window of process parameters, final stresses of the grown AlN layers spread over a wide range (with a pronounced tensile state), as mentioned in a previous study [33]. According to simple thermomechanic calculations, this contrast in stresses cannot be due to the temperature effect (expansion coefficient difference and initial misfit are of secondary importance and must both lead to compressive stresses at room temperature). This is confirmed by the absence of influence of temperature parameter on the responses related to stress. The only degree of freedom offered to explain such variability is the tensile stress due to the primary island coalescence. It allows the matching of all the measured stresses by involving islands sizes with sizes in the 10–50 nm range, in agreement with literature results [13,32,55] (see next section). The primary island nucleation is the main contributor to thin film stress when depositing AlN on sapphire. Moreover, the island size is strongly dependent on process parameters, so it can be managed. Some parameter effects on this response are rather simple to explain. For example the introduction of purge times between pulses allows surface diffusion of adatomes and leads to larger islands. Adding $AlCl_3$ prior deposition can also lead to a surface energy modification that increases island size. Increasing NH_3 flow rate gives the inverse effect, by blocking surface diffusion of aluminum species, which have a generally low diffusion coefficient. As the stress (through island size) is tunable by process parameters, it is even possible to decrease the tensile effect of nucleation and to deposit near-zero stress layers (at room temperature) by adjusting the recipe.

The effect of chlorination step parameters on island size (lamp furnace power and pellet size) seems difficult to explain as it appears that these parameters do not influence thickness (So chlorination step is not kinetically limiting the growth). However, if the chlorination step mainly generates $AlCl_3$, small amounts of $SiCl_4$ originating from silica walls of chlorination tube are also produced. Indeed, equilibrium thermodynamic calculations (Factsage 7.0, FACT database) indicate a gas mole fraction of about 1% $SiCl_4$ in $AlCl_3$ in the chlorination furnace conditions, released oxygen originating from silica etching being trapped into solid alumina form (on aluminum pellets). The fraction of this parasitic chloride depends on chlorination temperature, and is probably involved in surface energy effects explaining variation in nucleation island size. In the same idea, small or big pellets must modify the equilibrium in $SiCl_4$ by allowing more or less oxygen to be trapped into alumina form.

Second, the reactor used is cold-wall around the susceptor, essentially to avoid contamination of sample with species coming from the cold wall etching. It appears that it is a key particularity of

the process. Indeed, the effect of many parameters implies that a part of the reactants are condensed on the wall and released in an uncontrollable parasitic way. The effect of cooling down rate is the most representative: the slower the cooling rate (1%/min), the thicker the layer is. This can be only explained by a parasitic release of N and Al containing reactants from cooled walls that thicken the layer while cooling down. This is confirmed by the effect of hydrogen carrier gas flow rate. Increasing this flow rate from 500 to 1500 sccm increases the thickness despite a dilution effect, due to more efficient driving of reactants towards the substrate holder. This is also confirmed by the effect of hydrogen carrier gas on roughness. High growth rates and high roughness may have the same origin i.e., the increase of reactants fluxes for high hydrogen flow rate. Finally, increasing purge time also increases the thickness. Transient computational fluid dynamics modeling of the reactor (not given here) excludes the possibility of a surface limited growth effect (growth stops completely after 0.5 s from the beginning of purge period). Uncontrolled growth due to the release of wall condensates during purges is then the main cause of thickness increase.

In the same idea, cooling down under nitrogen decreases the surface roughness. Gas phase diffusion coefficient of reactive species in nitrogen is much lower than in hydrogen (5 times). Transport of species from cold walls to substrate by diffusion is reduced in nitrogen atmosphere. The roughness is noticeably lowered by the inhibition of parasitic growth during cooling down. In the next section another confirmation of the drawback of cold wall reactors will be given. It is worth noting that (whitish) deposits are formed during deposition in the cold upper part of the chlorination tube (solid $AlCl_3$), and around the cooled part of the reactor tube close to susceptor. Cold wall reactors should limit sample contamination (decrease of wall etching) but parasitic condensation and release is responsible for many other drawbacks.

Finally, the detrimental effect of purge time (from 0 to 4 s) must be explained. It was expected that adding purge time would facilitate the surface diffusion of adsorbed species. This effect is observed on island size during the first moments of growth (increasing purge time increases island size), which is logical. The effect on final roughness is inverse: increasing purge time surprisingly leads to rougher layers. It could be emphasized that purge time is efficient at the beginning of the growth, when the reactor walls and chlorination tube are cleaned, and becomes more and more detrimental for deposition on long times, when parasitic release of reactants becomes a noticeable source of growth for AlN. When reactor walls become covered with condensates, purge time is just an uncontrolled period of growth, when the N/Al ratio in gas phase (obviously unknown, but probably N-rich, as increasing NH_3 flow rate has the same effect as purge time) may lead to poor surface diffusion of adsorbed species.

These results partially explain lack of influence of parameters on crystal quality. It appears that the cold wall leads to condensation and release of parasitic species ($AlCl_3$, NH_4Cl, and the $AlCl_3.NH_3$ adduct) that participate to growth in an uncontrollable way.

Correlations between responses are now proposed to confirm these hypotheses and propose further process improvements.

5. Correlation between Responses

It is difficult to assess from the available literature whether small or large islands are desirable for a better quality of AlN layers. Small islands increase the tensile contribution of stress in the film, which is not desirable a priori. The influence of the nucleation island sizes on the propagation or annihilation of threading dislocations in III-V epitaxy is still debated in literature [56,57].

The DOE method has the obvious advantage of providing a huge number of experimental data collected in an extended experimental space and associated with their statistical significance (21 experiments). Figure 3 presents the island size deduced from Raman shift versus island size calculated from curvature. The standard deviation is indicated.

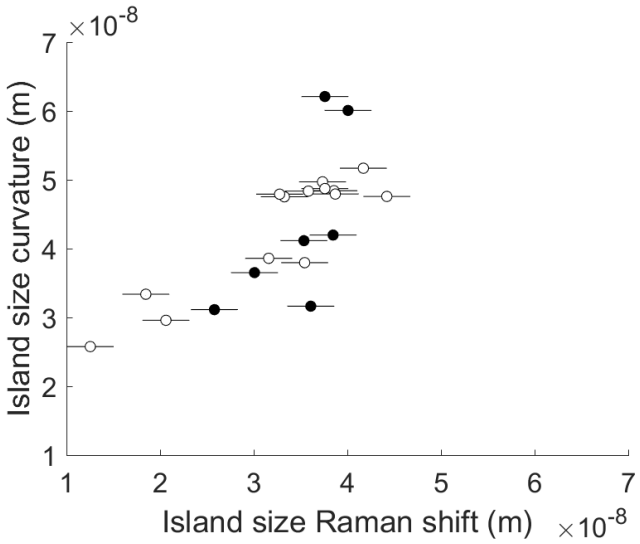

Figure 3. Island size deduced from Raman shift versus island size deduced from curvature. Full dots indicate samples with cracks. Standard deviation is indicated in both directions.

From Figure 3, we can observe that there is a rather good agreement between both source of data (Raman shift or curvature) used to calculate the primary nucleation island size, in particular if cracked samples are excluded from the discussion. It is worth noting that cracked samples and non-cracked samples do not form two distinct populations. Globally, the sizes of islands deduced from Raman shift are smaller on average, indicating that some tensile contribution of coalescence step during growth is partially lost at large scales. So we should admit that curvature, although easy to measure, reflects only partially the growth mechanisms.

It can be expected that epitaxial layers with near zero stress can be the best one. Figure 4 presents the crystal quality plotted versus the stress deduced from Raman shift measured on AlN samples.

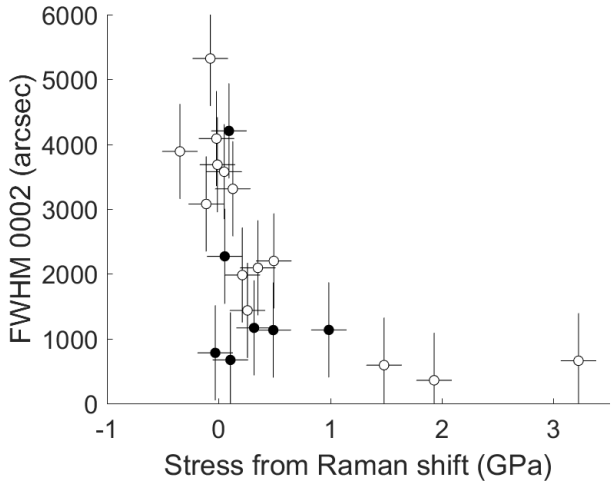

Figure 4. Crystal quality in AlN layers versus stress deduced from Raman shift. Full dots indicate samples with cracks. Standard deviation is indicated.

It is clear by observing Figure 4 that the more tensile the stress, the better the crystal quality. This plot could be transformed into the crystal quality as function of island sizes (Figure 5), which overcome the (weak) influence of deposition temperature. From Figure 5 it can be concluded that smaller nucleation islands lead to better crystal quality in the range of investigated parameters. It appears that the trend is particularly clear for the non-cracked samples (empty dots).

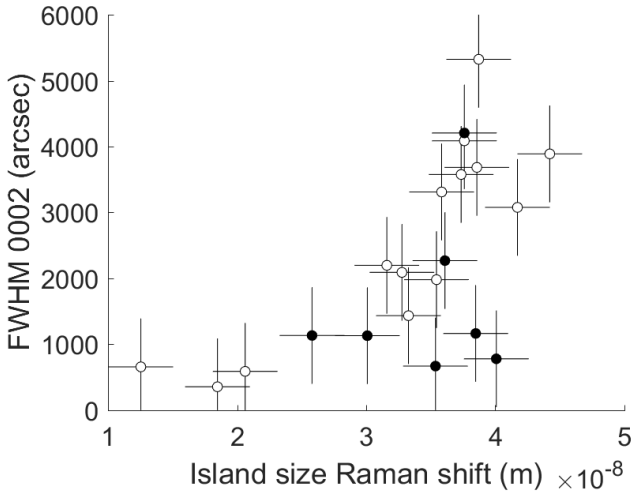

Figure 5. Nucleation island sizes deduced from Raman shift versus crystal quality. Full dots indicate sample with cracks. Standard deviation is indicated.

So we can conclude that within the range of parameters tested, small nucleation islands or strong tensile stresses are correlated with good quality of AlN layers. This conclusion strengthens the results of Balaji et al. [13,32,55] showing that low temperature nucleation layer (so small nucleation islands with high surface density) prior to epitaxial growth of AlN could be beneficial for improving crystal quality.

Moreover, this correlation is not an artifact due to parasitic growth as island coalescence is a very early phenomenon that appears when the reactor walls are still clean. Further parasitic growth can just randomly add noise to this correlation by modifying the final crystal quality only. So if recipe parameters do not play a major role on crystal quality, the size of islands does.

Figure 6 shows the average size of islands found in this study and the data of [48] and [13,55] plotted versus temperature. It can be noticed a good agreement and a logical trend: the higher the temperature, the larger are the nucleation islands. The huge error bar in this work is due to the fact that 14 parameters are varied in addition to temperature in this study. Some of them are very effective on island sizes, compared to temperature, which finally plays a minor role.

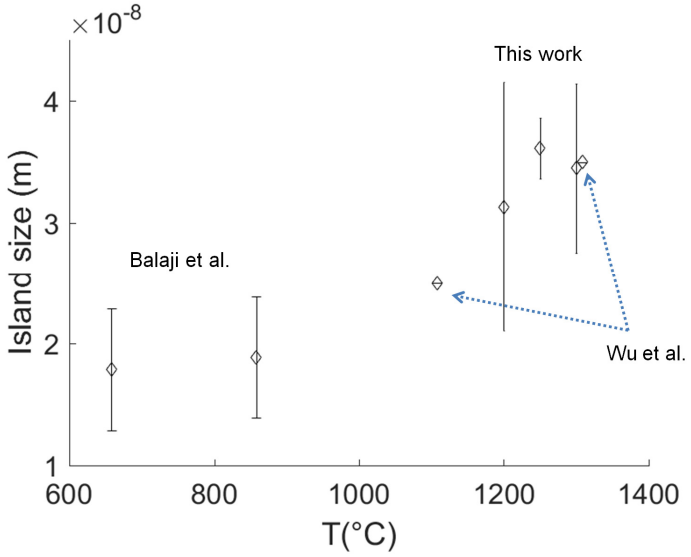

Figure 6. Nucleation island sizes versus temperature from references [13,48,55] and averaged from this work. Standard deviation is indicated when possible to estimate.

Finally, we can plot crystal quality (i.e., FWHM values of X-ray rocking curves for tilt component) versus thickness to assess if any kinetic mechanism of dislocation reduction (healing) exists in the layers as stated for III-V epitaxial growth [51]. Figure 7 presents the crystal quality versus the thickness. An opposite trend is observed—the thicker is the film, the lower is the crystal quality of AlN.

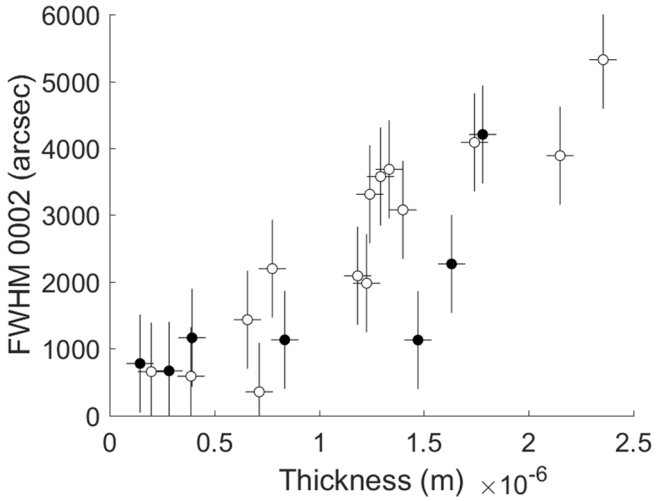

Figure 7. Crystal quality versus thickness of the AlN layer. Full dots indicate sample with cracks. Standard deviation is indicated.

The parasitic phenomenon already discussed, as an uncontrolled growth during cooling down by the release of wall condensates may be responsible. At least, annealing or dislocation reduction mechanisms related to thickness increase do not play a major role in these experimental recipes and reactor design within the range of tested parameters.

According to the DOE presented using the cold wall HVPE reactor depicted in Figure 1, we can give some final engineering recommendations and guidelines for CVD users:

- Cold wall reactors must have controlled wall temperature, as high as possible with available cooling fluid to avoid condensation and uncontrolled release of species.
- Robust method must be used to reveal driving growth parameters. Uncontrolled or considered as secondary parameters can overtake the recipe parameters. None of the growth parameters in CVD should be considered as secondary.
- CVD deposited layers can present very contrasted stress states that are mainly related to the coalescence step. Control of the early steps of growth is critical for stress management in grown layers, but also for aiming a good crystal quality.

6. Summary

We have assessed the performance of a cold wall HT-HVPE process by using a DOE approach for AlN growth. It allows the quantification of the experimental errors. It was shown that the crystal quality is not influenced by the classical process parameters but certainly influenced by condensation of reactive species on cold walls. It is more clearly correlated to nucleation island size. It was also demonstrated that experimental error must be quantified as parasitic effects can overtake the effects of recipe parameters. The next step of the method is to make a new DOE starting from the best working point defined in this study (sample of experiment #19) and involving new parameters like cold wall temperature, heating blanket temperature or degassing procedure in order to reveal all the first order parameters of the process influencing crystal quality. Then, a classical optimization work with surface response can be done, focused on only few leading parameters. It is expected that this robust method

will inspire CVD community to better understand and interpret growth results and to delimitate the effects process parameters and reactor design.

Acknowledgments: This work was supported by the French ANR research program EPICEA ANR-14-CE07-0008, "On Pillars" Epitaxial Overgrowth of Freestanding AlN Layers. The authors want to thank the University of Canterbury, New Zealand, for its collaboration by student exchange.

Author Contributions: Raphaël Boichot and Frédéric Mercier conceived and designed the experiments, based on preceding experimental data obtained by Gaël Giusti, conceived the modeling for island size calculation and wrote the article. Danying Chen was the main experimenter. She was trained by Mikhail Chubarov on the CVD apparatus and helped for structural characterizations and data treatment. Francis Baillet was the DOE expert that helped Raphaël Boichot with statistical exploitation of the data. DOE data were cross-validated with Matlab and Design Expert softwares. Gaël Giusti and Thomas Coughlan wrote the numerical code for island size calculation and validated its robustness on pre-existing experimental data with two programming language : Matlab and Python. Michel Pons did the computational fluid dynamics calculations for simulating the kinetics into the CVD reactor. He also helped for broad literature review. The choice of parameters and outputs involved in the DOE study was validated by the whole team.

Conflicts of Interest: The authors declare no conflict of interest.

References

1. Strite, S.; Morkoç, H. GaN, AlN, and InN: A review. *J. Vac. Sci. Technol. B Microelectron. Nanometer Struct.* **1992**, *10*, 1237–1266. [CrossRef]
2. Peng, B.; Gong, D.; Zhang, W.; Jiang, J.; Shu, L.; Zhang, Y. Effects of sputtering parameters on AlN film growth on flexible hastelloy tapes by two-step deposition technique. *Materials* **2016**, *9*, 686. [CrossRef] [PubMed]
3. Aissa, K.A.; Elmazria, O.; Boulet, P.; Aubert, T.; Legrani, O.; Mangin, D. Investigations of AlN thin film crystalline properties in a wide temperature range by in situ X-ray diffraction measurements: Correlation with AlN/Sapphire-based SAW structure performance. *IEEE Trans. Ultrason. Ferroelectr. Freq. Control* **2015**, *62*, 1397–1402. [CrossRef] [PubMed]
4. Kano, K.; Arakawa, K.; Takeuchi, Y.; Akiyama, M.; Ueno, N.; Kawahara, N. Temperature dependence of piezoelectric properties of sputtered AlN on silicon substrate. *Sens. Actuators A Phys.* **2006**, *130–131*, 397–402. [CrossRef]
5. Kinoshita, T.; Hironaka, K.; Obata, T.; Nagashima, T.; Dalmau, R.; Schlesser, R.; Moody, B.; Xie, J.Q.; Inoue, S.; Kumagai, Y.; et al. Deep-ultraviolet light-emitting diodes fabricated on AlN substrates prepared by hydride vapor phase epitaxy. *Appl. Phys. Express* **2012**, *5*, 122101. [CrossRef]
6. Sun, M.S.; Zhang, J.C.; Huang, J.; Wang, J.F.; Xu, K. AlN thin film grown on different substrates by hydride vapor phase epitaxy. *J. Cryst. Growth* **2016**, *436*, 62–67. [CrossRef]
7. Zhang, D.; Liu, F.M.; Yao, Y.; Yang, X.A. AlN epilayers and nanostructures growth in a homebuilt alumina hot-wall high temperature chemical vapor deposition system. *J. Mater. Sci. Mater. Electron.* **2014**, *25*, 2210–2219. [CrossRef]
8. Hartmann, C.; Wollweber, J.; Sintonen, S.; Dittmar, A.; Kirste, L.; Kollowa, S.; Irmscher, K.; Bickermann, M. Preparation of deep UV transparent AlN substrates with high structural perfection for optoelectronic devices. *Cryst. Eng. Comm.* **2016**, *18*, 3488–3497. [CrossRef]
9. Matsubara, H.; Mizuno, K.; Takeuchi, Y.; Harada, S.; Kitou, Y.; Okuno, E.; Ujihara, T. Direct growth of AlN single crystal on sapphire by solution growth method. *Jpn. J. Appl. Phys.* **2013**, *52*, 08JE17. [CrossRef]
10. Fukuyama, H.; Kato, M.; You, Y.; Ohtsuka, M. Growth mechanism of AlN crystals via thermal nitridation of sintered Al_2O_3-ZrO_2 plates. *Ceram. Int.* **2016**, *42*, 5153–5159. [CrossRef]
11. Soomro, A.M.; Wu, C.P.; Lin, N.; Zheng, T.C.; Wang, H.C.; Chen, H.Y.; Li, J.C.; Li, S.P.; Cai, D.J.; Kang, J.Y. Modified pulse growth and misfit strain release of an AlN heteroepilayer with a Mg-Si codoping pair by MOCVD. *J. Phys. D Appl. Phys.* **2016**, *49*, 115110. [CrossRef]
12. Boichot, R.; Claudel, A.; Baccar, N.; Milet, A.; Blanquet, E.; Pons, M. Epitaxial and polycrystalline growth of AlN by high temperature CVD: Experimental results and simulation. *Surf. Coat. Technol.* **2010**, *205*, 1294–1301. [CrossRef]

13. Balaji, M.; Claudel, A.; Fellmann, V.; Gelard, I.; Blanquet, E.; Boichot, R.; Pierret, A.; Attal-Tretout, B.; Crisci, A.; Coindeau, S.; et al. Effects of AlN nucleation layers on the growth of AlN films using high temperature hydride vapor phase epitaxy. *J. Alloys Compd.* **2012**, *526*, 103–109. [CrossRef]
14. Nagashima, T.; Kubota, Y.; Kinoshita, T.; Kumagai, Y.; Xie, J.Q.; Collazo, R.; Murakami, H.; Okamoto, H.; Koukitu, A.; Sitar, Z. Structural and optical properties of carbon-doped AlN substrates grown by hydride vapor phase epitaxy using AlN substrates prepared by physical vapor transport. *Appl. Phys. Express* **2012**, *5*, 125501. [CrossRef]
15. Kumagai, Y.; Kubota, Y.; Nagashima, T.; Kinoshita, T.; Dalmau, R.; Schlesser, R.; Moody, B.; Xie, J.Q.; Murakami, H.; Koukitu, A.; et al. Preparation of a freestanding AIN substrate from a thick AIN layer grown by hydride vapor phase epitaxy on a bulk AIN substrate prepared by physical vapor transport. *Appl. Phys. Express* **2012**, *5*, 055504. [CrossRef]
16. Takada, K.; Nomura, K.; Togashi, R.; Murakami, H.; Koukitu, A.; Kumagai, Y. Formation mechanism of AlN whiskers on sapphire surfaces heat-treated in a mixed flow of H_2 and N_2. *Jpn. J. Appl. Phys.* **2016**, *55*, 05FF01. [CrossRef]
17. Liu, X.-H.; Zhang, J.-C.; Su, X.-J.; Huang, J.; Zheng, S.-N.; Hu, Y.-Y.; Ye, B.-B.; Zhao, J.-J.; Wang, J.-F.; Zhang, J.-P.; et al. Fabrication of crack-free AlN film on sapphire by hydride vapor phase epitaxy using an in situ etching method. *Appl. Phys. Express* **2016**, *9*, 045501. [CrossRef]
18. Tojo, S.; Yamamoto, R.; Tanaka, R.; Thieu, Q.T.; Togashi, R.; Nagashima, T.; Kinoshita, T.; Dalmau, R.; Schlesser, R.; Murakami, H.; et al. Influence of high-temperature processing on the surface properties of bulk AlN substrates. *J. Cryst. Growth* **2016**, *446*, 33–38. [CrossRef]
19. Chen, G.; Jia, S.; Wang, P.; Zhang, H.; Zhang, H.; Zhang, B.; Wang, X.; Zhang, J. Simulation of self-developed vertical HVPE system for growth of aluminium nitride. *Mater. Res. Innov.* **2014**, *18*, 1062–1067. [CrossRef]
20. Huang, J.; Niu, M.T.; Zhang, J.C.; Wang, W.; Wang, J.F.; Xu, K. Reduction of threading dislocation density for AlN epilayer via a highly compressive-stressed buffer layer. *J. Cryst. Growth* **2017**, *459*, 159–162. [CrossRef]
21. Lee, G.S.; Lee, C.; Jeon, H.; Lee, C.; Bae, S.G.; Ahn, H.S.; Yang, M.; Yi, S.N.; Yu, Y.M.; Lee, J.H.; et al. Growth of AlN layer on patterned sapphire substrate by hydride vapor phase epitaxy. *Jpn. J. Appl. Phys.* **2016**, *55*, 05FC02. [CrossRef]
22. Baker, T.; Mayo, A.; Veisi, Z.; Lu, P.; Schmitt, J. High temperature HVPE of AlN on sapphire templates. In *Physica Status Solidi C: Current Topics in Solid State Physics*; Eddy, C.R., Kuball, M., Koleske, D.D., Amano, H., Eds.; Wiley-VCH Verlag Gmbh: Weinheim, Germany, 2014; Volume 11, pp. 373–376.
23. Katagiri, Y.; Kishino, S.; Okuura, K.; Miyake, H.; Hiramatu, K. Low-pressure HVPE growth of crack-free thick AlN on a trench-patterned AlN template. *J. Cryst. Growth* **2009**, *311*, 2831–2833. [CrossRef]
24. Wu, P.; Funato, M.; Kawakami, Y. Environmentally friendly method to grow wide-bandgap semiconductor aluminum nitride crystals: Elementary source vapor phase epitaxy. *Sci. Rep.* **2015**, *5*, 17405. [CrossRef] [PubMed]
25. Sun, M.; Zhang, J.; Huang, J.; Li, X.; Wang, L.; Liu, X.; Wang, J.; Xu, K. Influence of thickness on strain state and surface morphology of AlN grown by HVPE. *J. Semicond.* **2016**, *37*, 123001. [CrossRef]
26. Tran, B.T.; Hirayama, H.; Maeda, N.; Jo, M.; Toyoda, S.; Kamata, N. Direct growth and controlled coalescence of thick AlN template on micro-circle patterned Si substrate. *Sci. Rep.* **2015**, *5*, 14734. [CrossRef] [PubMed]
27. Gordon, L.; Varley, J.B.; Lyons, J.L.; Janotti, A.; Van de Walle, C.G. Sulfur doping of AlN and AlGaN for improved n-type conductivity. *Phys. Status Solidi Rapid Res. Lett.* **2015**, *9*, 462–465. [CrossRef]
28. Zhang, D.; Liu, F.M.; Cai, L.G. Structure, optical spectra and biaxial stress of (0002) AlN epilayers grown on c-sapphire by high-temperature chemical vapor deposition. *Phys. Status Solidi A Appl. Mater. Sci.* **2014**, *211*, 2394–2402. [CrossRef]
29. Raghavan, S.; Redwing, J.M. In situ stress measurements during the MOCVD growth of AlN buffer layers on (111) Si substrates. *J. Cryst. Growth* **2004**, *261*, 294–300. [CrossRef]
30. Chubarov, M.; Mercier, F.; Lay, S.; Charlot, F.; Crisci, A.; Coindeau, S.; Encinas, T.; Ferro, G.; Reboud, R.; Boichot, R. Growth of aluminum nitride on flat and patterned Si (111) by high temperature halide CVD. *Thin Solid Films* **2017**, *623*, 65–71. [CrossRef]
31. Abadias, G.; Guerin, P. In situ stress evolution during magnetron sputtering of transition metal nitride thin films. *Appl. Phys. Lett.* **2008**, *93*, 111908. [CrossRef]

32. Balaji, M.; Ramesh, R.; Arivazhagan, P.; Jayasakthi, M.; Loganathan, R.; Prabakaran, K.; Suresh, S.; Lourdudoss, S.; Baskar, K. Influence of initial growth stages on AlN epilayers grown by metal organic chemical vapor deposition. *J. Cryst. Growth* **2015**, *414*, 69–75. [CrossRef]
33. Boichot, R.; Coudurier, N.; Mercier, F.; Lay, S.; Crisci, A.; Coindeau, S.; Claudel, A.; Blanquet, E.; Pons, M. Epitaxial growth of AlN on c-plane sapphire by high temperature hydride vapor phase epitaxy: Influence of the gas phase N/Al ratio and low temperature protective layer. *Surf. Coat. Technol.* **2013**, *237*, 118–125. [CrossRef]
34. Kitagawa, S.; Miyake, H.; Hiramatsu, K. High-quality AlN growth on 6H-SiC substrate using three dimensional nucleation by low-pressure hydride vapor phase epitaxy. *Jpn. J. Appl. Phys.* **2014**, *53*, 05FL03. [CrossRef]
35. Zhuang, Q.Q.; Lin, W.; Yang, W.H.; Yang, W.C.; Huang, C.C.; Li, J.C.; Chen, H.Y.; Li, S.P.; Kang, J.Y. Defect suppression in AlN epilayer using hierarchical growth units. *J. Phys. Chem. C* **2013**, *117*, 14158–14164. [CrossRef]
36. Endres, D.; Mazumder, S. Numerical investigation of pulsed chemical vapor deposition of aluminum nitride to reduce particle formation. *J. Cryst. Growth* **2011**, *335*, 42–50. [CrossRef]
37. Zhang, D.; Liu, F.M.; Cai, L.G. Investigation, characterization and effect of substrate position on thick AlN layers grown by high temperature chemical vapor deposition. *J. Mater. Sci. Mater. Electron.* **2015**, *26*, 1239–1245. [CrossRef]
38. Claudel, A.; Fellmann, V.; Gelard, I.; Coudurier, N.; Sauvage, D.; Balaji, M.; Blanquet, E.; Boichot, R.; Beutier, G.; Coindeau, S.; et al. Influence of the V/III ratio in the gas phase on thin epitaxial AlN layers grown on (0001) sapphire by high temperature hydride vapor phase epitaxy. *Thin Solid Films* **2014**, *573*, 140–147. [CrossRef]
39. Conroy, M.; Zubialevich, V.Z.; Li, H.N.; Petkov, N.; Holmes, J.D.; Parbrook, P.J. Epitaxial lateral overgrowth of AlN on self-assembled patterned nanorods. *J. Mater. Chem. C* **2015**, *3*, 431–437. [CrossRef]
40. Boichot, R.; Coudurier, N.; Mercier, F.; Claudel, A.; Baccar, N.; Milet, A.; Blanquet, E.; Pons, M. CFD modeling of the high-temperature HVPE growth of aluminum nitride layers on c-plane sapphire: From theoretical chemistry to process evaluation. *Theor. Chem. Acc.* **2014**, *133*, 1419. [CrossRef]
41. Bryan, I.; Bryan, Z.; Mita, S.; Rice, A.; Tweedie, J.; Collazo, R.; Sitar, Z. Surface kinetics in AlN growth: A universal model for the control of surface morphology in III-nitrides. *J. Cryst. Growth* **2016**, *438*, 81–89. [CrossRef]
42. Pons, M.; Boichot, R.; Coudurier, N.; Claudel, A.; Blanquet, E.; Lay, S.; Mercier, F.; Pique, D. High temperature chemical vapor deposition of aluminum nitride, growth and evaluation. *Surf. Coat. Technol.* **2013**, *230*, 111–118. [CrossRef]
43. Segal, A.S.; Bazarevskiy, D.S.; Bogdanov, M.V.; Yakovlev, E.V. Modeling analysis of AlN and AlGaN HVPE. In *Physica Status Solidi C: Current Topics in Solid State Physics*; Butte, R., Ed.; Wiley-VCH Verlag Gmbh: Weinheim, Germany, 2009; Volume 6, pp. S329–S332.
44. Li, Z.; Zhang, J.; Li, J.; Jiang, H.; Fu, X.; Han, Y.; Xia, Y.; Huang, Y.; Yin, J.; Zhang, L.; et al. Modeling and simulation of a novel susceptor composed of two materials in MOVPE reactor. *J. Cryst. Growth* **2014**, *402*, 175–178. [CrossRef]
45. Nyutu, E.K.; Suib, S.L. Experimental design in the deposition of BN interface coatings on SiC fibers by chemical vapor deposition. *Surf. Coat. Technol.* **2006**, *201*, 2741–2748. [CrossRef]
46. Hsueh, C.H.; Lee, S.; Lin, H.Y. Analyses of mode I edge delamination by thermal stresses in multilayer systems. *Compos. Part B* **2006**, *37*, 1–9. [CrossRef]
47. Raghavan, S.; Redwing, J. Intrinsic stresses in AlN layers grown by metal organic chemical vapor deposition on (0001) sapphire and (111) Si substrates. *J. Appl. Phys.* **2004**, *96*, 2995–3003. [CrossRef]
48. Wu, B.; Bai, J.; Tassev, V.L.; Nakarmi, M.L.; Sun, W.; Huang, X.; Dudley, M.; Zhang, H.; Bliss, D.F.; Lin, J.; et al. Stress evolution during the early stages of AlN vapor growth. *Mater. Res. Soc. Symp. Proc.* **2006**, *892*, 653.
49. Reeber, R.R.; Wang, K. Lattice parameters and thermal expansion of important semiconductors and their substrates. *Mater. Res. Soc. Symp. Proc.* **2000**, *622*. [CrossRef]
50. Vodenitcharova, T.; Zhang, L.C.; Zarudi, I.; Yin, Y.; Domyo, H.; Ho, T.; Sato, M. The effect of anisotropy on the deformation and fracture of sapphire wafers subjected to thermal shocks. *J. Mater. Process. Technol.* **2007**, *194*, 52–62. [CrossRef]

51. Ayers, E. *Heteroepitaxy of Semiconductors, Theory, Growth and Characterization*; CRC Press: Boca Raton, FL, USA, 2007.
52. Saint Gobain Crystals. Available online: http://www.crystals.saint-gobain.com/uploadedFiles/SG-Crystals/Documents/sapphire-material-products-properties.pdf (accessed on 27 July 2017).
53. Yang, S.; Miyagawa, R.; Miyake, H.; Hiramatsu, K.; Harima, H. Raman scattering spectroscopy of residual stresses in epitaxial AlN films. *Appl. Phys. Express* **2011**, *4*, 031001. [CrossRef]
54. Davydov, V.Y.U.; Kitaev, Y.U.E.; Goncharuk, I.N.; Smirnov, A.N.; Graul, J.; Semchinova, O.; Uffmann, D.; Smirnov, M.B.; Mirgorodsky, A.P.; Evarestov, R.A. Phonon dispersion and Raman scattering in hexagonal GaN and AlN. *Phys. Rev. B* **1998**, *58*, 12899–12907. [CrossRef]
55. Balaji, M.; Claudel, A.; Fellmann, V.; Gélard, I.; Blanquet, E.; Boichot, R.; Coindeau, S.; Roussel, H.; Pique, D.; Baskar, K.; et al. Significance of initial stages on the epitaxial growth of AlN using high temperature halide chemical vapor deposition. *Phys. Status Solidi C* **2012**, *9*, 511–514. [CrossRef]
56. Moram, M.A.; Ghedia, C.S.; Rao, D.V.S.; Barnard, J.S.; Zhang, Y.; Kappers, M.J.; Humphreys, C.J. On the origin of threading dislocations in GaN films. *J. Appl. Phys.* **2009**, *106*, 073513. [CrossRef]
57. Kamber, D.S.; Wu, Y.; Haskell, B.A.; Newman, S.; DenBaars, S.P.; Speck, J.S.; Nakamura, S. Direct heteroepitaxial growth of thick AlN layers on sapphire substrates by hydride vapor phase epitaxy. *J. Cryst. Growth* **2006**, *297*, 321–325. [CrossRef]